Dynamical quantum-electrodynamics embedding: Combining time-dependent density functional theory and the near-field method

Yi Gao and Daniel Neuhauser[a)]
Department of Chemistry and Biochemistry, University of California at Los Angeles, Los Angeles, California 90095-1569, USA

(Received 11 June 2012; accepted 31 July 2012; published online 21 August 2012)

We develop an approach for dynamical ($\omega > 0$) embedding of mixed quantum mechanical (QM)/classical (or more precisely QM/electrodynamics) systems with a quantum sub-region, described by time-dependent density functional theory (TDDFT), within a classical sub-region, modeled here by the recently proposed near-field (NF) method. Both sub-systems are propagated simultaneously and are coupled through a common Coulomb potential. As a first step we implement the method to study the plasmonic response of a metal film which is half jellium-like QM and half classical. The resulting response is in good agreement with both full-scale TDDFT and the purely classical NF method. The embedding method is able to describe the optical response of the whole system while capturing quantum mechanical effects, so it is a promising approach for studying electrodynamics in hybrid molecules-metals nanostructures. © *2012 American Institute of Physics*. [http://dx.doi.org/10.1063/1.4745847]

I. INTRODUCTION

Optical properties of metal nanostructures are a focus of nanoscience in the recent decade due to wide applications in various disciplines. The responses of metallic nanostructures at sub-wavelength scales are dominated by localized surface plasmon resonances (LSPR), i.e., the collective oscillation of valence electrons in metals. These plasmonic currents exhibit various novel dynamical phenomena, such as surface enhanced Raman scatterings (SERS),[1–3] single photon emissions,[4,5] plasmon-exciton hybridization,[6–8] and dynamical electron transfer or charge separation between adsorbed molecules and substrates.[9,10] Further, we earlier predicted that the molecular dipoles can even guide plasmonic currents.[11,12] These features led to the emergence of a new field, labeled nanopolaritonics or molecular plasmonics.

Modeling nanopolaritonics requires the combination of the electrodynamics of nanostructures and associated molecules. The LSPR in metallic nanostructures is usually studied with classical electrodynamics, either analytically, e.g., with Mie theory[13,14] and plasmon hybridization model,[15,16] or numerically, typically with finite-difference time domain (FDTD),[17,18] or the discrete dipole approximations.[19–21] Recently, we proposed the near-field (NF) method[22] for studying the optical response of nanostructures at sub-wavelength scales. The NF is essentially a time-dependent Poisson equation method, and solves the Maxwell equations with the approximation that the electric field is longitudinal and retardation effects are negligible. The method has been successfully applied to study the optical response of metallic nanostructures at sub-wavelength scales and has been extended to include an arbitrary number of dielectrics.[23]

Although the optical responses of nanostructures can be described by classical electrodynamics, the electronic dynamics in molecule can only be correctly studied by quantum mechanics. Recently, *ab initio* calculations such as time-dependent density functional theory (TDDFT) have been performed to understand the plasmonic coupling between metallic nanostructures and molecule-metallic hybrid nanostructure systems,[24–28] revealing the importance of quantum effect at sub-nanometer contacting regime. However, due to numerical constraints, only nanostructures involving hundreds of atoms have been computationally studied, sizes beyond ~2 nm are not accessible by fully quantum methods. To bridge the gap between different sizes in the molecule-nanostructure system, various approaches have been developed. The general strategy is to treat the molecular system as quantum mechanical while the metallic nanostructure is classically described. To list a few, Masiello and Schatz developed a many-body theory on SERS processes;[29] they also reported a numerical approach combining TDDFT and FDTD methods to study the enhanced absorption of molecules adsorbed on metal surface.[30,31] Jensen *et al.* have developed an atomistic electrodynamics[32] model and coupled it with TDDFT, which has been used to study the relation between optical response of a hybrid system and molecule-metal separation and adsorption orientations.[33] Recently, we have also developed different models to couple electrodynamics with molecule described by a two-level quantum system.[12,34–37]

An alternative solution proposed here is embedding, i.e., the interface region, including both adsorbed molecule and nearby finite metal cluster, is described by full-fledged quantum mechanical approach; while the rest of the nanostructure is treated as classical or described by some less accurate quantum mechanical (QM) model. The idea is analogous to embedding methods in electronic structure.[38–40] The goal of the embedding here is to obtain correct optical response of the

a)dxn@chem.ucla.edu.

 © 2012 American Institute of Physics

hybrid nanometer sized system, while capturing the static and dynamic quantum effects of coupling between molecule and metal substrate.

The specific dynamical embedding proposed here combines a time-dependent quantum mechanical propagation (in practice TDDFT) with NF. The embedding is very simple since in NF the dynamics is non-retarded and is determined only by a longitudinal electric field, due to an overall electric potential, just as in typical quantum (i.e., most TDDFT) descriptions. By sharing the common potential which is calculated from both embedded region and the rest of the NF region, the two subsystems interact and propagate simultaneously. Using this embedding scheme the optical response of a large multi-scale system is correctly captured at a reasonable computational cost. The resulting TDDFT-NF embedding approach is promising for the study of nanopolaritonics effect, as well as the electrodynamics enhancement and chemical enhancement in SERS and other combined photonics-materials effects.

Here we present the general approach and a first implementation, the plasmon response of a thin metal film. The general formalism is given in Sec. II. We then implement the method in a metallic thin film slab which is half-QM and half-NF (Sec. III). Finally discussion and conclusions follow in Sec. IV.

II. GENERAL METHODOLOGY

We first describe the general methodology and in Sec. III specialize to a model one-dimensional (1D) system.

There are two regions, a quantum mechanical one described here by DFT and TDDFT, and a classical one described by electrodynamics – here, specifically, by the NF approach, which is the long wavelength limit of the time-dependent Maxwell equations. We start with NF and then turn to TDDFT. Afterwards, we describe the embedding, which has two facets: both the connecting potential through a single potential related to the overall densities, and also the relation between the parameters used and the initial static state. Atomic units ($e = \hbar = m_e = 1$) are used.

A. Time-dependent NF equations

The classical part is handled here by NF, a time-dependent Poisson algorithm. It relates the charge density in the classical region to a polarization,

$$\rho_{\mathrm{NF}}(\mathbf{r},t) = -\nabla\cdot\mathbf{P}(\mathbf{r},t), \tag{1}$$

which in turn is related to the electric field. In the frequency domain the relation is

$$\tilde{\mathbf{P}}(\mathbf{r},\omega) = (\epsilon(\mathbf{r},\omega)-\epsilon_0)\,\tilde{\mathbf{E}}(\mathbf{r},\omega), \tag{2}$$

where in practice a Lorentzian expansion is used to describe the dielectric permittivity,

$$\epsilon(\mathbf{r},\omega) = \epsilon_\infty(\mathbf{r}) + \sum_{j=1}^{N_j}\frac{\epsilon_0\beta_j(\mathbf{r})}{\bar{\omega}_j^2(\mathbf{r}) - i\alpha_j(\mathbf{r})\omega - \omega^2}. \tag{3}$$

Here, N_j ranges typically from $\bar{\omega}^2$, depending on the material and the level of sophistication needed, while ϵ_∞, β_j, $\bar{\omega}_j$, and α_j are Lorentzian-oscillator fitting parameters. (Note that $\mathbf{P}$ is not the full polarization, which has an additional component $(\epsilon_\infty(\mathbf{r})-\epsilon_0)\mathbf{E}(\mathbf{r},\omega)$, associated with the frequency-independent part of the permittivity; however, that component is accounted for by the way the Poisson equation is solved.)

Equation (2) is then transformed (as in FDTD) to the time domain with auxiliary quantities $\mathbf{P}_j$ for each oscillator,

$$\mathbf{P}(\mathbf{r},t) = \sum_{j=1}^{N_j}\mathbf{P}_j(\mathbf{r},t), \tag{4}$$

$$\frac{d^2}{dt^2}\mathbf{P}_j(\mathbf{r},t) = -\alpha(\mathbf{r})\frac{d}{dt}\mathbf{P}_j(\mathbf{r},t) - \bar{\omega}_j^2(\mathbf{r})\mathbf{P}_j(\mathbf{r},t) + \epsilon_0\beta_j(\mathbf{r})\mathbf{E}(\mathbf{r},t). \tag{5}$$

In NF, the electric field is assumed longitudinal, and is then related to the overall electrostatic potential

$$\begin{aligned}\mathbf{E}(\mathbf{r},t) &= -\nabla\phi(\mathbf{r},t) + \mathbf{E}_{\mathrm{ext}}(\mathbf{r},t)\\ &= -\nabla\phi(\mathbf{r},t) + \mathbf{E}_{\mathrm{ext},0}(\mathbf{r})\,\delta(t),\end{aligned} \tag{6}$$

where we introduced an external field $\mathbf{E}_{\mathrm{ext},0}$, typically a pulse with a uniform spatial distribution (delta function in time).

For a classical-only description, the potential is determined from the NF charge density ρ_{NF}. However, anticipating the embedding in the next stage, we note that the Coulomb potential for electrons needs to be obtained from a Poisson equation relating the potential to the overall charge density, which yields

$$\begin{aligned}-\nabla\cdot(\epsilon_\infty(\mathbf{r})\nabla\phi(\mathbf{r},t)) &= \rho_{\mathrm{tot}}(\mathbf{r},t)\\ -\nabla\cdot(\epsilon_\infty(\mathbf{r})\mathbf{E}_{\mathrm{ext},0}(\mathbf{r}))\delta(t),\end{aligned} \tag{7}$$

with the total charge defined as

$$\rho_{\mathrm{tot}}(\mathbf{r},t) = -n(\mathbf{r},t) + \rho_b(\mathbf{r}) + \rho_{\mathrm{NF}}(\mathbf{r},t). \tag{8}$$

Here, $n(\mathbf{r},t)$ is the electronic number density due to the quantum (DFT) region, and ρ_b is the ionic background density. This simple Poisson relation is the central connection for the embedding.

The initial conditions for the NF equations, before the application of the pulse, are a stationary polarization and electric field. This is obtained from the static forms of the equations above (Eqs. (4)–(8)), yielding

$$\mathbf{P}_{j,0}(\mathbf{r}) = \frac{\epsilon_0\beta_j(\mathbf{r})}{\bar{\omega}_j^2(\mathbf{r})}\mathbf{E}_0(\mathbf{r}), \tag{9}$$

so

$$\mathbf{P}_0(\mathbf{r}) = \left(\epsilon_\infty(\mathbf{r}) - \epsilon_0 + \epsilon_0\sum_{j=1}^{N_j}\frac{\beta_j(\mathbf{r})}{\bar{\omega}_j^2(\mathbf{r})}\right)\mathbf{E}_0(\mathbf{r}), \tag{10}$$

and

$$\rho_{\mathrm{NF},0}(\mathbf{r}) = -\nabla\cdot\mathbf{P}_0(\mathbf{r}), \tag{11}$$

where

$$-\nabla\cdot\left(\epsilon_\infty\left(\mathbf{r}\right)\nabla\phi_0\left(r\right)\right)\equiv-n_0\left(\mathbf{r}\right)+\rho_b\left(\mathbf{r}\right)+\rho_{\mathrm{NF},0}\left(\mathbf{r}\right), \tag{12}$$

and the subscript "0" on the densities and fields refers to the static period before the pulse application.

B. DFT and TDDFT

The quantum region is treated through the time-dependent TDDFT equations for a set of orbitals, $\Psi_m(\mathbf{r},\,t)$:

$$i\frac{\partial}{\partial t}\Psi_m\left(\mathbf{r},t\right)=\left(-\frac{1}{2}\nabla^2+v_{\mathrm{eff}}\left(\mathbf{r},t\right)\right)\Psi_m\left(\mathbf{r},t\right), \tag{13}$$

where v_{eff}, the time-dependent effective potential, is the sum of an electrostatic and an exchange-correlation (XC) part,

$$v_{\mathrm{eff}}\left(\mathbf{r},t\right)=-\phi\left(\mathbf{r},t\right)+v_{\mathrm{xc}}\left(\mathbf{r},t\right). \tag{14}$$

The electrostatic part is obtained by the solution of the Poisson equation, Eq. (7); it involves a quantum number density, $n(\mathbf{r},\,t)$ obtained in TDDFT from the occupied orbitals:

$$n\left(\mathbf{r},t\right)=2\sum_m\left|\Psi_m\left(\mathbf{r},t\right)\right|^2. \tag{15}$$

The dependence of the XC potential on the charge density is uncertain, especially when embedding is used; here we choose the simplest approach where the exchange correlation functional is the usual adiabatic XC functional of the instantaneous electric density, $v_{\mathrm{xc}}\left(\mathbf{r},t\right)=\delta E_{\mathrm{xc}}/\delta n\left(\mathbf{r},t\right)$, but other options will be explored in the future.

The initial conditions for the orbitals, before the application of the pulse, is that they solve the time-independent Kohn-Sham equation,

$$E_m\Psi_{m,0}\left(\mathbf{r}\right)=\left(-\frac{1}{2}\nabla^2+v_{\mathrm{eff}}\left(\mathbf{r}\right)\right)\Psi_{m,0}\left(\mathbf{r}\right). \tag{16}$$

Here, as in the latter time-dependent evolution,

$$v_{\mathrm{eff}}\left(r\right)=-\phi_0\left(r\right)+v_{\mathrm{xc}}\left(r\right), \tag{17}$$

and Eq. (12) relates the densities to the potential, with

$$n_0(\mathrm{r})=2\sum_m\left|\Psi_{m,0}\left(r\right)\right|^2. \tag{18}$$

The electronic structure of the hybrid system is calculated iteratively until the self-consistent Eqs. (9)–(12) and (16)–(18) are converged. At convergence, the static dipole moment, which is a combination of a quantum and NF parts, is

$$\mathbf{d}_{\mathrm{tot},0}=\mathbf{d}_{\mathrm{QM},0}+\mathbf{d}_{\mathrm{NF},0}\equiv\int\left(\rho_b\left(\mathbf{r}\right)-n_0\left(\mathbf{r}\right)\right)\mathbf{r}d\mathbf{r}+\int\mathbf{P}_0\left(\mathbf{r}\right)d\mathbf{r}. \tag{19}$$

C. Time propagation

After convergence of the static quantities a pulse is applied and the combined NF and TDDFT equations are solved simultaneously. Previously, we have presented the leap-frog approach to propagating the NF equations, so we only briefly review it here. We define the current densities as

$$\mathbf{J}_j\left(\mathbf{r},t\right)=\frac{\partial\mathbf{P}_j(\mathbf{r},t)}{\partial t}. \tag{20}$$

Then, the initial conditions on the time-dependent propagations are (in a slight variation on the previous formalism, designed to allow for simple application of the delta-function pulse at $t=0$):

$$\mathbf{P}_j\left(\mathbf{r},t=-\Delta t\right)=\mathbf{P}_{j0}\left(\mathbf{r}\right),$$

$$\mathbf{J}_j\left(\mathbf{r},t=-\frac{\Delta t}{2}\right)=0.$$

The leap-frog algorithm is then

$$\mathbf{P}_j\left(\mathbf{r},t+\Delta t\right)=\mathbf{P}_j\left(\mathbf{r},t\right)+\Delta t\mathbf{J}_j\left(\mathbf{r},t+\frac{\Delta t}{2}\right), \tag{21}$$

$$\mathbf{J}_j\left(\mathbf{r},t+\frac{\Delta t}{2}\right)=\frac{1-\frac{\alpha_j}{2}\Delta t}{1+\frac{\alpha_j}{2}\Delta t}\mathbf{J}_j\left(\mathbf{r},t-\frac{\Delta t}{2}\right)-\frac{\Delta t}{1+\frac{\alpha_j}{2}\Delta t}\times\left(\bar{\omega}_j^2\mathbf{P}_j\left(\mathbf{r},t\right)-\epsilon_0\beta_j\left(\mathbf{r}\right)\mathbf{E}\left(\mathbf{r},t\right)\right), \tag{22}$$

and $\mathbf{E}(\mathbf{r},\,t=n\Delta t)$ and $\phi(\mathbf{r},\,t=n\Delta t)$ are obtained by solving Eqs. (6)–(8), with $\delta(t)$ replaced by $\delta_{n0}/\Delta t$.

In conjunction, the Kohn-Sham orbitals are also propagated; the simplest way is through a split operator (though other approaches are also feasible) such as, in loose notation:

$$\Psi_m\left(\mathbf{r},t+\Delta t\right)=e^{-iv_{\mathrm{eff}}(\mathbf{r},t)\Delta t/2}e^{-iK dt}e^{-iv_{\mathrm{eff}}(\mathbf{r},t)\Delta t/2}\Psi_m\left(\mathbf{r},t\right). \tag{23}$$

Here, v_{eff} is both time- and space-dependent (we use the usual LDA adiabatic potential), and K is the kinetic energy operator. Other possible variants include self-consistent (forward-backward) propagations, etc.; these will be discussed in a future publication.

The result of the calculation can be summarized in the overall time-dependent induced dipole, defined as

$$\delta\mathbf{d}_{\mathrm{tot}}\left(t\right)=\delta\mathbf{d}_{\mathrm{QM}}\left(t\right)+\delta\mathbf{d}_{\mathrm{NF}}\left(t\right)\equiv\int\left(\rho_b\left(\mathbf{r},t\right)-n\left(\mathbf{r},t\right)\right)\mathbf{r}d\mathbf{r}-\mathbf{d}_{\mathrm{QM},0}+\int\mathbf{P}\left(\mathbf{r},t\right)d\mathbf{r}-\mathbf{d}_{\mathrm{NF},0}. \tag{24}$$

The optical absorption coefficient, $\sigma_{abs}(\omega)$, is determined from imaginary part of the dynamical polarizability in the frequency domain,

$$\sigma_{abs}\left(\omega\right)\equiv\frac{4\pi\omega}{c}\mathrm{Im}\,\alpha\left(\omega\right)=\frac{4\pi\omega}{c}\mathrm{Im}\left(\frac{\delta\mathbf{d}\left(\omega\right)\cdot\hat{\mathbf{E}}_{\mathrm{ext},0}}{\left|\hat{\mathbf{E}}_{\mathrm{ext},0}\right|}\right). \tag{25}$$

where

$$\delta\mathbf{d}\left(\omega\right)\equiv\int e^{i\omega t}\delta\mathbf{d}_{\mathrm{tot}}\left(t\right)dt. \tag{26}$$

D. Parameter consistency

Beyond the overall theme of using a single Coulomb potential based on the combined density or Eq. (8), the remaining issues are the division of space to classical and quantum regions, and the relation between the parameters used for $\epsilon(\mathbf{r}, \omega)$ and the DFT functionals.

We first discuss the division to two parts. We envision a small QM region, and a classical region which encompasses it. The division between the two is through a dividing function, $f(\mathbf{r})$, so that

$$\rho_{\mathrm{b}}(\mathbf{r}) = f(\mathbf{r})\,\bar{\rho}_b(\mathbf{r}), \tag{27}$$

and

$$\beta_j(\mathbf{r}) = (1 - f(\mathbf{r}))\,\bar{\beta}_j(\mathbf{r}), \tag{28}$$

where $\bar{\rho}_b$ is the density which would have been used if a purely QM description was used throughout the whole region, and analogously $\bar{\beta}_j$ is the Lorentzian-oscillator strength coefficient which would have been used if a purely classical NF description was taken. The dividing function, $f(\mathbf{r})$, is mostly 1 (for the QM region) or 0 (classical region), and varies rapidly but continuously in a small QM/classical interface region. The reason for Eqs. (27) and (28) is that the Lorentzian oscillators, if taken as physically motivated quantities, are proportional to the classical charge density, so that using f and $1 - f$ gives a smooth transition from a classical to a quantum charge density. (Future work will examine the detailed dependence on the smoothness parameter of the dividing function f but in our simulations the results were barely dependent on the details of f as long as it varies from 0 to 1 over less than 3 a.u.)

Next, consider the relation between the DFT and electrodynamics parameters. For embedding to be successful, we require that at least long wavelength excitations ($q \to 0$) should have equal effects in both the classical and quantum regions; put differently, this requires that

$$\bar{\epsilon}_{\mathrm{DFT}}(\mathbf{q} \to 0, \omega > 0) = \epsilon(\mathbf{q} \to 0, \omega > 0), \tag{29}$$

where $\bar{\epsilon}_{\mathrm{DFT}}$ is a bulk QM index of refraction associated with the region near the border of the quantum mechanical region, and the right hand side refers to the electrodynamics (NF here) index of refraction. Typically the embedding will be done over a piece of metal so that $\bar{\epsilon}_{\mathrm{DFT}}$ refers to the metal.

Note that the equations above imply that one should ideally not mix an experimentally derived susceptibility with an arbitrary DFT exchange-correlation (or exchange-correlation-memory) functional, but instead either fit QM to an experimentally derived $\epsilon(\mathbf{q} = 0, \omega > 0)$; or, as done here, replace the experimental electrodynamics susceptibility by one which is designed to fit the QM susceptibility.

E. Jellium slab

The following discusses the embedding for a simplest case where near the edges of the QM region the nuclear potential is constant (i.e., the border of the QM region is a metal with a jellium potential). We emphasize that jellium is just a special case; the discussion above is general, and more sophisticated descriptions of the metal (with more complicated indices of refraction than the jellium's) are feasible. Further, the jellium needs only be used near the edge, and within the quantum regions any potential (such as molecular) could be used.

In the jellium-metal case, $\bar{\rho}_{\mathrm{b}}(\mathbf{r}) = \rho_0$ near the edge of the QM (DFT) region. The limit of the metallic susceptibility at large wavelength in that region is

$$\chi_{\mathrm{jellium,DFT}}(\mathbf{q} = 0, \omega > 0) = -\frac{\omega_p^2}{\omega^2}, \tag{30}$$

so that for the classical subsystem, the metal is described here by the dielectric permittivity of a single ($N_j = 1$) dissipationless ($\alpha_j = 0$) Lorentzian oscillator:

$$\epsilon(\mathbf{r}, \omega) = \epsilon_0\left(1 + \frac{\beta(\mathbf{r})}{\bar{\omega}^2 - \omega^2}\right), \tag{31}$$

so

$$\epsilon_\infty(\mathbf{r}) = \epsilon_0,$$

and also

$$\beta(\mathbf{r}) = (1 - f(\mathbf{r}))\,g(\mathbf{r})\,\beta_0,$$

and

$$\beta_0 = 4\pi\rho_0.$$

Here, $g(\mathbf{r})$ is the shape function of the overall structure. Note that we have introduced a small restoring force part through a $\bar{\omega}^2$ parameter; this is necessary for proper self-consistency, so that Eq. (10) can be solved for the initial polarization. Further, the sign of this $\bar{\omega}^2$ parameter is necessary for numerical convergence of the initial conditions (see Sec. III) and its introduction is acceptable since our interest is only at high frequencies and not in the static susceptibility so the modification of the index of refraction at low frequencies will not affect the dynamical results. We have numerically checked that the results are not influenced by the magnitude of $\bar{\omega}$ as long as it is sufficiently small.

We note that Eqs. (9)–(12) show that in the static (prepulse) case there is still an induced electron density in the classical region due to the density profile in the quantum region. The induced electron density in the classical region is

$$\begin{aligned}\rho_{\mathrm{NF}}(\mathbf{r}) &= -\nabla\cdot\mathbf{P}_0(\mathbf{r}) = -\nabla\cdot\{(\epsilon(\mathbf{r}, 0) - \epsilon_0)\,\mathbf{E}_0(\mathbf{r})\} \\ &= -\nabla\cdot\left(\frac{\epsilon_0\beta(\mathbf{r})}{\bar{\omega}^2}\nabla\phi_0(\mathbf{r})\right),\end{aligned} \tag{32}$$

and the Coulomb potential is evaluated directly by convolution, since here $\epsilon_\infty(\mathbf{r}) = \epsilon_0$:

$$\phi(\mathbf{r}) = \frac{1}{4\pi\epsilon_0}\int\frac{\rho_{\mathrm{NF}}(\mathbf{r}') + \rho_{\mathrm{b}}(\mathbf{r}') - n_0(\mathbf{r}')}{|\mathbf{r} - \mathbf{r}'|}d\mathbf{r}'. \tag{33}$$

III. TEST-CASE: ONE-DIMENSIONAL JELLIUM SLAB

A. One-dimensional formulation

To keep the system simple, we implement the embedding method to study the plasmonic response of a metal film. The film is modeled as half quantum mechanical (jellium background) and half classical. The jellium extends between $-L$

$< z < 0$, and the classical NF half between $0 < z < L$. In our previous notation, the shape of the film is $g(z) = 1$ for $|z| < L$, and 0 otherwise.

We used a Fermi-Dirac-like transfer function, $f(z)$, which changes from 1 in the quantum region ($z < 0$) to 0 in the positive region, and its width is labeled as σ. The 1D equations are very similar to the 3D counterpart; the only difference is that, since the Hamiltonian is only z-dependent, the time-dependent 3D orbitals are reduced to 1D quantum well states ψ_n fulfilling

$$\left(-\frac{1}{2}\frac{d^2}{dz^2} + v_{\text{eff}}(z)\right)\psi_n(z,t) = \frac{i\partial}{\partial t}\psi_n(z,t), \tag{34}$$

which are normalized as $\int dz\,|\psi_n(z,t)|^2 = 1$, while the three-dimensional density, obtained by integrating the x-y wave-vector, is then as usual

$$n(z,t) = \frac{1}{\pi}\sum_n^{\varepsilon_n < E_F}(E_{\text{F}} - \epsilon_n)\,|\psi_n(z,t)|^2. \tag{35}$$

The rest of the equations proceed as before. We assume that the system is perturbed by a constant longitudinal optical field pulse $E_{\text{ext}}(r,t) = E_{\text{ext},0}\delta(t)\mathbf{z}$, so that the one-dimensional Poisson equation is solved directly from

$$-\frac{d^2}{dz^2}\phi(z,t) = \frac{\rho_b(z) + \rho_{\text{NF}}(z,t) - n(z,t)}{\epsilon_0} \tag{36}$$

(the term involving the divergence of the constant external filed times the polarization in Eq. (6) vanishes).

B. Numerical results

For the 1D test case, we implemented the embedding approach to study the optical response of a metal slab with jellium density of $\rho_0 = 0.08$ (correspondingly, $r_s = 3.0$ and $\beta_0 = 0.11$) and thickness $2L = 120$ (recall that a.u. units are used throughout). A Fermi-Dirac function $f(z) \sim 1/\left(1 + \exp\left(-\frac{z}{2\sigma}\right)\right)$ is used for smooth separation of the quantum and halves, with $\sigma = 1.0$ a.u. The resulting structure of the hybrid system is illustrated in Fig. 1. Since 1D periodic boundary conditions are used along the z direction, a large simulation region of 600 a.u. is employed, guaranteeing the elimination of inter-cell interaction. A total number of 512 grid points are used, giving a grid spacing $\Delta z = 1.17$ a.u. which is sufficient to ensure convergence. A Lorentzian-oscillator parameter $\bar{\omega} = 0.041$ is used to model the metal in the NF region.[41–44]

Figure 2 gives the calculated static charge density distributions, both quantum mechanical and NF. The electron density of the QM jellium region at $z \sim -L$, the vacuum-QM interface, shows a Friedel oscillation, which is in exact agreement with that obtained by using a full QM jellium calculations for the whole film. At the QM-NF interface ($z \sim 0$), the distribution is smooth since we adopted a smooth positive background, although the decay depths are different for electrons and the jellium background. Also, at the QM-NF interface, the classical charge distribution established a dipole layer pointing from the QM to the NF regions, which almost

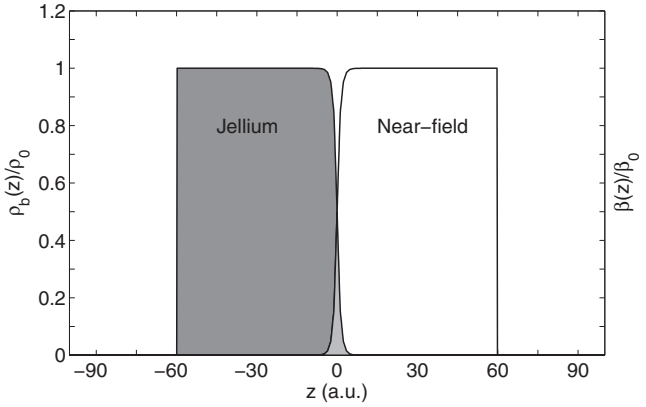

FIG. 1. Schematics of embedding approach for metal slab with thickness 120 a.u. The left half is modeled by jellium and quantum mechanical (QM) description, while the right half is studied with near-field (NF) method. The transition from the quantum to classical regions is artificially smoothed in the figure, i.e., in practice it is much more abrupt, around 2 a.u.

balances the dipole created by $\rho_b(z) - n_0(z)$; the total charge density then gives rise to an almost vanishing dipole layer at $z \sim 0$. The resulting total charge distribution shows that the embedding interface, or QM-NF transition region has little effect on the electronic structure at vacuum-QM interface.

Once the static quantities are produced, we proceed to the time-dependent simulations. As this is a first implementation, we are not trying to employ an efficient TDDFT approach so a small time step ($\Delta t = 0.025$ a.u.) is used. Note that a major advantage of the NF approach, the possibility of using large steps, is lost now since the QM simulations dictate a small step; however, NF is still convenient to use in the embedding since it is potential-based, and, further, future simulations will employ more sophisticated TDDFT propagation schemes with larger time steps.

An external delta-function pulse $E_{\text{ext}}(r, t = 0) = \frac{1}{\Delta t}E_0\mathbf{z}$ is applied and at $t > 0$ the external field vanishes. A small initial delta-function field strength is used ($E_0 = 10^{-5}$ a.u.)

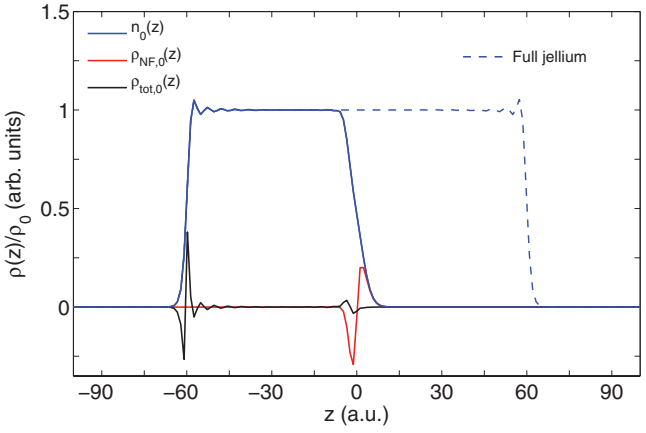

FIG. 2. Static charge distributions of the hybrid system. The jellium or QM electron density (solid blue line) $n_0(z)$ shows a Friedel oscillation at the vacuum-jellium interface, in exact agreement with that obtained from a full QM calculation (dashed blue line). While the NF density (solid red line) $\rho_{\text{NF},0}(z)$ established a static non-vanishing dipole at the jellium-NF interface, which approximately balances the dipole built by $\rho_b(z) - n_0(z)$. The total static charge distribution $\rho_{\text{tot},0}(z)$ is also given (solid black line).

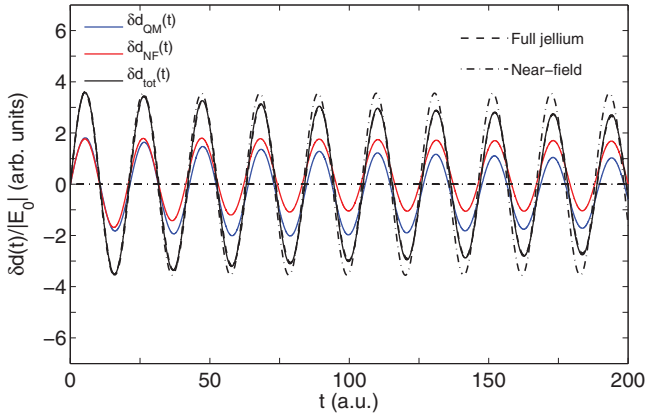

FIG. 3. Normalized dynamical induced dipole strength obtained by embedding method. The total dipole strength and the contributions from QM electrons and the NF subsystem are all displayed. The embedding result is in agreement with that calculated using either full QM TDDFT (dashed line) or classical NF method (dotted-dashed line).

to ensure that the response is linear. Equations (21)–(23) are propagated for 80.0 fsec (∼2000 a.u.).

Figure 3 gives the calculated time-dependent induced dipole moment per area per the external electric field of the hybrid QM-NF system. The total dipole oscillates with a period of ∼20 a.u. The figure also shows the dipole component due to the QM electrons and the NF part. Initially, each component contributed half of the total dipole moment of the hybrid system, consistent with our division of the system as half QM and half classical. Latter, there is a slight shift between the components.

In Figure 2 we have also performed full QM TDDFT and classical NF calculations for the whole film with thickness of 2*L* for comparison. The simulations show that the dipole in the hybrid system is almost indistinguishable from the full QM TDDFT result, and they differ from the NF oscillation since the classical dipole is an exact sinusoidal function of time without dephasing. The non-constant amplitude of the dipole in either hybrid or full QM systems is due to the energy transfer between plasmons and electron-hole pairs.

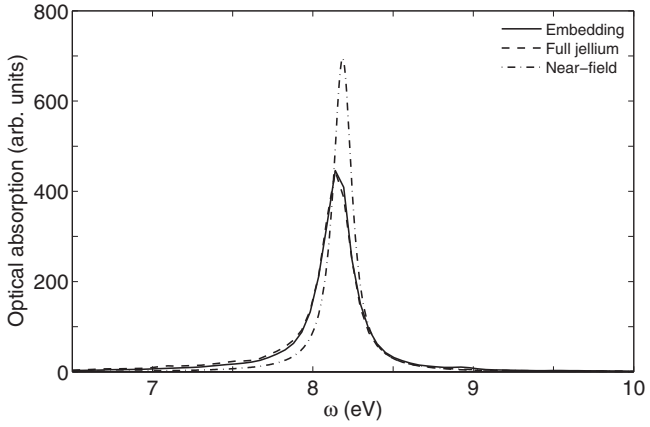

FIG. 4. Frequency-dependent optical absorption of the hybrid system (solid line). The spectra obtained by using full QM TDDFT (dashed line) and classical NF calculation (dotted-dashed line) are given for comparison.

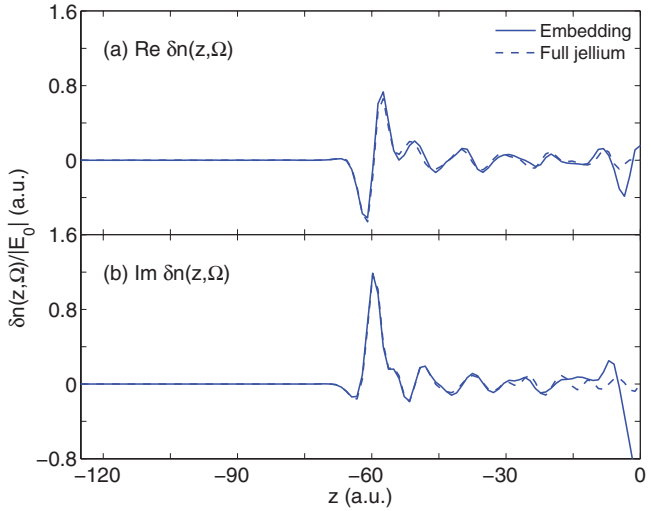

FIG. 5. (a) Real and (b) imaginary part of frequency-dependent 1D induced QM electron density $\delta n(z, \Omega)$, in which Ω is the resonance frequency. The results obtained by using hybrid system (solid blue lines) are compared with those using full QM calculations (dashed blue lines).

The obtained time-dependent dipole moments are converted into frequency-dependent optical absorption spectrum, as given in Fig. 4. A decay function of the form $e^{-t/\eta}$ is used for all three systems to broaden the spectra, with $\eta = 400$ a.u. This plot quantifies the physical process shown in Fig. 3, i.e., the plasmon resonance in the hybrid system produces that in the full QM jellium system. Comparing the hybrid system and full QM jellium film, both the plasmon frequency and spectral shape are almost the same. Compared with classical-only NF spectrum, the optical absorption of the hybrid system is not as sharp as that obtained using a classical-only NF calculation. This is due to that fact that the classical model involves no damping for the plasmon resonance. In addition, the plasmon resonance energy in the hybrid system is red-shifted with respect to the classical result; this is due to the spill-out effect of the QM electrons at the vacuum-jellium interface, so that the effective electron density participating in the plasmon resonance is lowered.

This picture is corroborated in Fig. 5, in which the dynamical induced QM electron densities are investigated. The distribution obtained from the hybrid system again coincides with that calculated using the full QM jellium model, demonstrating that the spatial properties also reproduced by the embedding approach. Thus, the embedding scheme successfully gives overall correct electrodynamics of the whole system combining QM jellium and classical NF sub-ones.

IV. DISCUSSION AND CONCLUSIONS

Although the system we have studied is as simple as 1D and jellium-like, the formalism is general and can be directly extended to 3D systems, and the whole system can be arbitrarily divided into sub-systems of two different descriptions.

In practice, there will be considerations such as the best shape of the transition function, $f(\mathbf{r})$; a smoother function will reduce the static dipole in the interface region and lead to closer match between the fully quantum and embedding

dipole. Further, for realistic descriptions it will be advisable to introduce memory and damping potentials such that the TDDFT response will be guided by the experimental values that determine the NF Lorentzian-oscillator parameters, instead of the opposite route taken here. Future works will also tackle the issue of modification of the functionals to account for the presence of the NF region.

In the embedding approach, the QM sub-region only shares a common Coulomb potential, thus the QM methods used for this region is most naturally a potential based method, such as DFT or TDDFT. More elaborate QM descriptions can be adopted. These include correlated wave-function methods (e.g., configuration interaction), but they will also most likely be coupled through an overall potential.

The outlined modifications are only going to add to the overall framework, developed here, which should give quantitatively accurate results due to the two ingredients – the use of a common Coulomb potential, and the matching of the susceptibilities.

Finally, we note that the same overall approach is going to be applicable when other dynamical embedding schemes are applied; for example, our recent dynamical orbital-free density functional (OF-DFT) approach[45] could be used instead of the Maxwell relation, and has the added advantage that not only the long-wavelength susceptibilities are matched, but the whole $\epsilon(\mathbf{q}, \omega)$ is matched between the classical and quantum regions.

ACKNOWLEDGMENTS

We are grateful for support by the NSF (Grant Nos. CHE-0810003 and CHE-1112500). Discussions with Gang Lu and Roi Baer are gratefully acknowledged.

[1] S. Nie and S. R. Emory, Science **275**, 1102 (1997).
[2] K. Kneipp, M. Moskovits, and H. Kneipp, *Surface-Enhanced Raman Scattering: Physics and Applications* (Springer, Berlin/New York, 2006).
[3] L. Jensen, C. M. Aikens, and G. C. Schatz, Chem. Soc. Rev. **37**, 1061 (2008).
[4] D. E. Chang, A. S. Sorensen, P. R. Hemmer, and M. D. Lukin, Phys. Rev. Lett. **97**, 053002 (2006).
[5] D. E. Chang, A. S. Sorensen, E. A. Demler, and M. D. Lukin, Nat. Phys. **3**, 807 (2007).
[6] N. T. Fofang, T. H. Park, O. Neumann, N. A. Mirin, P. Nordlander, and N. J. Halas, Nano Lett. **8**, 3481 (2008).
[7] N. T. Fofang, N. K. Grady, Z. Y. Fan, A. O. Govorov, and N. J. Halas, Nano Lett. **11**, 1556 (2011).
[8] Y. B. Zheng, B. Kiraly, S. Cheunkar, T. J. Huang, and P. S. Weiss, Nano Lett. **11**, 2061 (2011).
[9] Y. Tian and T. Tatsuma, J. Am. Chem. Soc. **127**, 7632 (2005).
[10] X. M. Wu, E. S. Thrall, H. T. Liu, M. Steigerwald, and L. Brus, J. Phys. Chem. C **114**, 12896 (2010).
[11] C. Arntsen, K. Lopata, M. R. Wall, L. Bartell, and D. Neuhauser, J. Chem. Phys. **134**, 084101 (2011).
[12] D. Neuhauser, J. Chem. Phys. **135**, 204305 (2011).
[13] G. Mie, Ann. Phys. **25**, 377 (1908).
[14] C. F. Bohren and D. R. Huffman, *Absorption and Scattering of Light by Small Particles* (Wiley, New York, 1983).
[15] E. Prodan, C. Radloff, N. J. Halas, and P. Nordlander, Science **302**, 419 (2003).
[16] E. Prodan and P. Nordlander, J. Chem. Phys. **120**, 5444 (2004).
[17] K. L. Shlager and J. B. Schneider, IEEE Antennas Propag. Mag. **37**, 39 (1995).
[18] A. Taflove and S. C. Hagness, *Computational Electrodynamics: The Finite-Difference Time-Domain Method*, 3rd ed. (Artech House, Boston, 2005).
[19] B. T. Draine and P. J. Flatau, J. Opt. Soc. Am. A Opt. Image Sci. Vis **11**, 1491 (1994).
[20] W. H. Yang, G. C. Schatz, and R. P. Vanduyne, J. Chem. Phys. **103**, 869 (1995).
[21] M. A. Yurkin, A. G. Hoekstra, R. S. Brock, and J. Q. Lu, Opt. Express **15**, 17902 (2007).
[22] A. Coomar, C. Arntsen, K. A. Lopata, S. Pistinner, and D. Neuhauser, J. Chem. Phys. **135**, 084121 (2011).
[23] S. Li, Y. Gao, and D. Neuhauser, J. Chem. Phys. **136**, 234104 (2012).
[24] J. Zuloaga, E. Prodan, and P. Nordlander, Nano Lett. **9**, 887 (2009).
[25] D. C. Marinica, A. K. Kazansky, P. Nordlander, J. Aizpurua, and A. G. Borisov, Nano Lett. **12**, 1333 (2012).
[26] L. L. Zhao, L. Jensen, and G. C. Schatz, J. Am. Chem. Soc. **128**, 2911 (2006).
[27] S. M. Morton and L. Jensen, J. Am. Chem. Soc. **131**, 4090 (2009).
[28] P. Song, P. Nordlander, and S. Gao, J. Chem. Phys. **134**, 074701 (2011).
[29] D. J. Masiello and G. C. Schatz, Phys. Rev. A **78**, 042505 (2008).
[30] H. N. Chen, J. M. McMahon, M. A. Ratner, and G. C. Schatz, J. Phys. Chem. C **114**, 14384 (2010).
[31] J. Mullin and G. C. Schatz, J. Phys. Chem. A **116**, 1931 (2012).
[32] L. L. Jensen and L. Jensen, J. Phys. Chem. C **113**, 15182 (2009).
[33] S. M. Morton and L. Jensen, J. Chem. Phys. **135**, 134103 (2011).
[34] D. Neuhauser and K. Lopata, J. Chem. Phys. **127**, 154715 (2007).
[35] K. Lopata, D. Neuhauser, and R. Baer, J. Chem. Phys. **127**, 154714 (2007).
[36] K. Lopata and D. Neuhauser, J. Chem. Phys. **130**, 104707 (2009).
[37] K. Lopata and D. Neuhauser, J. Chem. Phys. **131**, 014701 (2009).
[38] N. Govind, Y. A. Wang, and E. A. Carter, J. Chem. Phys. **110**, 7677 (1999).
[39] C. Huang, M. Pavone, and E. A. Carter, J. Chem. Phys. **134**, 154110 (2011).
[40] J. M. Lastra, J. W. Kaminski, and T. A. Wesolowski, J. Chem. Phys. **129**, 074107 (2008).
[41] S. Link and M. A. Ei-Sayed, Annu. Rev. Phys. Chem. **54**, 331 (2003).
[42] S. A. Maier, *Plasmonics: Fundamentals and Applications* (Springer, New York, 2007).
[43] L. Novotny and B. Hecht, *Principles of Nano-Optics*, 2nd ed. (Cambridge University Press, Cambridge, 2012).
[44] N. J. Halas, Nano Lett. **10**, 3816 (2010).
[45] D. Neuhauser, S. Pistinner, A. Coomar, X. Zhang, and G. Lu, J. Chem. Phys. **134**, 144101 (2011).